crystals

MDPI

Article

Enhanced Ferromagnetism Induced by Chemical Doping and Epitaxial Strain in $La_{0.8}Sr_{0.2}CoO_3$ Films

Changzheng Xie [1], Zhijie Chen [1], Xinghua Wang [1], Ying Meng [1,*] and Yihao Wang [2,*]

[1] Universities Joint Key Laboratory of Photoelectric Detection Science and Technology in Anhui Province, School of Physics and Materials Engineering, Hefei Normal University, Hefei 230601, China
[2] Anhui Province Key Laboratory of Condensed Matter Physics at Extreme Conditions, High Magnetic Field Laboratory, HFIPS, Chinese Academy of Sciences, Hefei 230031, China
* Correspondence: mengying_2018@163.com (Y.M.); yihaow@hmfl.ac.cn (Y.W.)

Abstract: The perovskite $LaCoO_3$ and $La_{0.8}Sr_{0.2}CoO_3$ thin films were synthesized successfully by a polymer-assisted deposition method. The structural characterization and thermal decomposition measurements indicate that appropriately increasing the annealing temperature is helpful in improving the film crystallinity. Compared with $LaCoO_3$ films, the Curie temperature is enhanced to a higher temperature in $La_{0.8}Sr_{0.2}CoO_3$ films, which is attributed to the changes in both the valence state and spin state induced by the chemical doping. In addition, a broad transition temperature region is observed in $La_{0.8}Sr_{0.2}CoO_3$ films, revealing the existence of inhomogeneous ground states in this system.

Keywords: ferromagnetic perovskite; chemical doping; spin-state transition; lattice relaxation

check for updates

Citation: Xie, C.; Chen, Z.; Wang, X.; Meng, Y.; Wang, Y. Enhanced Ferromagnetism Induced by Chemical Doping and Epitaxial Strain in $La_{0.8}Sr_{0.2}CoO_3$ Films. *Crystals* **2023**, *13*, 623. https://doi.org/10.3390/cryst13040623

Academic Editors: Teng Ma and Lin Wang

Received: 12 March 2023
Revised: 28 March 2023
Accepted: 29 March 2023
Published: 4 April 2023

1. Introduction

Over the last decades, perovskite-type transition-metal oxides have attracted substantial attention because of their great potential in both fundamental studies and technological applications in new-generation spin-dependent quantum devices [1–4]. As a member of perovskite-type transition-metal oxides, $LaCoO_3$ (LCO) has been extensively studied due to its interesting spin-state transition and applications in fields, including catalysts [5], solar cells [6], etc. At low temperatures, the Co^{3+} ions in bulk LCO possess a $3d^6$ electron configuration of low-spin ($t_{2g}{}^6e_g{}^0$, S = 0) state. With increasing temperature, the spin-state transition occurs in two steps. First, the spin transforms from the low-spin state ($t_{2g}{}^6e_g{}^0$, S = 0) state to the intermediate-spin ($t_{2g}{}^5e_g{}^1$, S = 1) state around 100 K. Secondly, a change from the intermediate-spin state to a mixed state of the intermediate- and high- spin ($t_{2g}{}^4e_g{}^2$, S = 2) states happens at around 500 K. More importantly, a ferromagnetic transition around 85 K has been found in LCO films, while the LCO bulk samples are nonmagnetic [7–9]. Although ferromagnetism appears in LCO thin films, its exact origin of it remains unclear. Previously, some studies demonstrated that epitaxial strain induced by substrates plays an important role in the formation of ferromagnetic ordering in LCO thin films [10,11], while others proposed that oxygen vacancy formation was crucial for the occurrence of ferromagnetism [12,13]. Therefore, there are controversies in theory about the mechanism of ferromagnetism in LCO films. As two of the most important factors for determining the physical properties of LCO, the epitaxial strain and the oxygen vacancy are closely related to the lattice distortions and valence states of Co ions in samples.

Besides epitaxial strains and oxygen vacancy mentioned above, the lattice distortions and valence states of Co ions that could be induced by chemical doping provide another way to manipulate the physical properties and to explore the origin of ferromagnetism in perovskite LCO films [14–16]. At the same time, the ion doping changes the valence states of Co ions and further breaks the balance among the competing parameters, including

lattice, spin, charge, orbit, etc., leading to possible exotic behaviors in this system. Although the LCO films grown on different substrates have been extensively studied, less attention has been paid to make the effect of chemical strain in doped LCO thin film systems clear.

In this work, the influence of chemical strain on lattice distortion and ground state was studied in Sr-doped LCO films. The crucial effect of annealing temperature on the film crystal quality is also highlighted. The results will help to make the related mechanisms of ferromagnetism in the LCO system clear and optimize the epitaxial growth to obtain films with high quality. Herein, the pristine LCO and Sr-doped LCO thin films on $SrTiO_3$ substrates were obtained by a facile polymer-assisted deposition (PAD) technique [17]. The structure, surface topography and magnetic properties of $La_{1-x}Sr_xCoO_3$ (x = 0, 0.2) thin films are studied in detail. The results show that an appropriate increase in the annealing temperature is helpful in improving the crystallinity of $LaCoO_3$ films. The mechanism for improvements in the crystallinity of $LaCoO_3$ films was revealed by thermal decomposition measurements on the 50% PEI (polyethyleneimine). Because the ionic radius of Sr^{2+} is larger than that of La^{3+}, the *c*-axis lattice parameter of $La_{0.8}Sr_{0.2}CoO_3$ film is larger than that in LCO film. Therefore, the Sr doping results in the longer Co–O bond and further make the films favor the high-spin state instead of the low-spin one. In addition, the Sr doping will introduce Co^{4+} ($3d^5$) and bring about the double exchange interactions in the form of Co^{4+}–O–Co^{3+} configurations in $La_{0.8}Sr_{0.2}CoO_3$ films. The above two reasons are responsible for the higher ferromagnetic transition temperature in doped samples compared to that in LCO film. Moreover, a broad transition temperature region is observed in $La_{0.8}Sr_{0.2}CoO_3$ films, indicating the existence of inhomogeneous ground states in this system.

2. Experimental Details

LCO thin films and doping samples were fabricated by a polymer-assisted deposition technique. The precursor solution was received as follows. To begin, the high purity (≥99.99%) EDTA (Ethylene Diamine Tetraacetic Acid) of 0.2922 and 0.2922 g PEI (polyethyleneimine) with a molecular weight of 70,000 was dissolved in 10 mL H_2O. The mixture solution would be transparent after stirring for an hour, which is marked as solution A. The $La(NO_3)_3$, $Co(NO_3)_2$ and $Sr(NO_3)_2$ metal salts in a 4:5:1 molar ratio were dissolved in deionized water marked as solution B. Solution B was slowly added to solution A by a dropper, then the obtained mixing solution was stirred by a magnetic stirring apparatus for 10 h at room temperature, and then continued to be stirred in a 60 °C oil bath until the solution remaining was ~5 mL. The films were obtained via the dip-coating and thermal treatment process. The LCO thin films and doping samples were deposited on treated single-crystal (001), (011), and (111)-oriented $SrTiO_3$ (STO) substrates (10 × 5 × 0.5 mm) at 5000 rpm over 60 s by a spin coating technique, respectively. Then the coated substrates were placed in a muffle furnace. In order to avoid the formation of bubbles on the film surface, a low ramp rate of 0.5 °C min^{-1} was used from room temperature to 700 °C to make sure that the water was evaporated and PEI was burned up. The samples were then heated to a holding temperature at a rate of 5 °C min^{-1}. After keeping warm for two hours, the films were slowly cooled down to room temperature at a rate of 1 °C min^{-1}. We note that the heat treatment process for LCO films is different, which is mentioned in the first paragraph of the results and discussion section. In general, the chemical composition and doping amount of the epitaxial perovskite films are consistent with the molar ratio of the metal salts in raw materials. In this study, the atomic ratio of La and Sr in raw materials is 4:1. Hence the doped sample is referred to as $La_{0.8}Sr_{0.2}CoO_3$ throughout the paper. In addition, the raw materials mentioned here were all purchased from Aladdin Co., Ltd. (Shanghai, China).

The structural characterizations of the films, including $\theta/2\theta$ symmetric scan, ω-scan (rocking curve) as well as in-plane φ-scan, were performed by a Rigaku TTRIII X-ray diffractometer (XRD, Rigaku Company, Tokyo, Japan) with Cu K_α radiation (=1.54187Å). The thermal stability was studied by differential scanning calorimetry coupled with thermal gravimetric analysis. Measurements were performed on the SDT-Q600 with an airflow

(TA Instruments Company, New Castle, DE, USA). The LCO precursor with a volume of 3 mL was heated to 1073 K at a rate of 10 K min^{-1}. The morphological properties of the deposited LCO were observed by atomic force microscopy (AFM, Auto Probe Pc; in contact mode, with low-stress silicon nitride tip of less than 200 Å radius, Bruker Company, Billerica, MA, USA). All the images were obtained with a scanning area of 5.0 × 5.0 μm. Moreover, the morphological characteristics of the LCO films are also obtained by an FEI Sirion 200 field emission scanning electron microscope (SEM, FEI Company, Eindhoven, Netherlands). In addition, the magnetic properties of the films were investigated via a Quantum Design MPMS-7 superconducting quantum interference device (SQUID, Quantum Design Company, San Diego, CA, USA) magnetometer. The field-cooled (FC) magnetization was measured in the temperature range 10 K $\leq T \leq$ 300 K with an external magnetic field of H = 100Oe applied parallel to the film surface.

3. Results and Discussion

3.1. Structural and Morphological Characteristics of LCO Films

In general, the thermal treatment process is crucial for the growth process and crystal quality of epitaxial films [18]. In this part, the studies about structural characteristics of LCO grown on (001) with different annealing temperatures were carried out to study the influence of annealing temperature on film quality. The polymeric LCO films were annealed in an air atmosphere with temperatures of 500, 600, 700, 800 and 900 °C, respectively. The XRD $\theta/2\theta$ symmetric scans were performed on the LCO films to characterize the sample qualities. As shown in Figure 1, the XRD patterns exhibit two sets of peaks, representing the (002) diffraction peak of LCO and substrate, respectively. It is obvious that the peaks of LCO films shift to higher angles with the annealing temperature rising from 500 °C to 900 °C. According to Bragg's law, the out-of-plane c-axis lattice parameters c_{film} of LCO films are calculated and shown in Table 1. It is obvious that the c_{film} decreases with increasing annealing temperature. According to the previous report on $LaMnO_3$ thin films, this behavior is attributed to the fewer oxygen defects in samples annealed at higher temperatures [19]. Fewer oxygen defects mean higher cobalt valence with a smaller ionic radius, leading to the lattice contraction along the *c*-axis. At the same time, with the increase in annealing temperature, the relative intensity of (002) diffraction peaks gradually increases, and the peak width decreases. This behavior indicates a better crystallization of films with higher annealing temperatures.

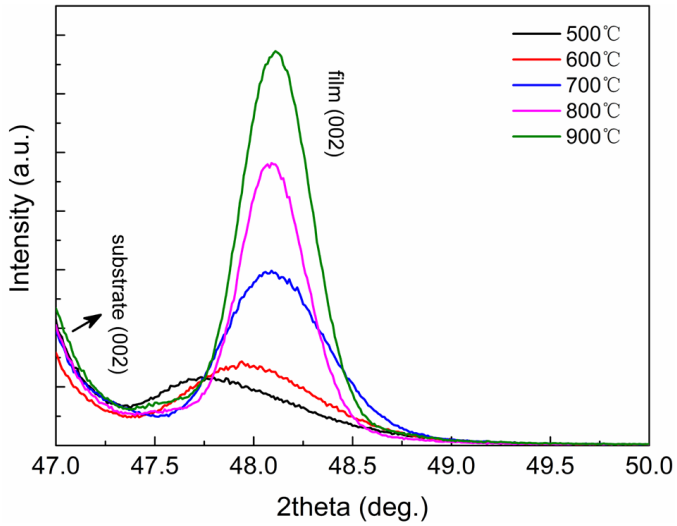

Figure 1. (Color online) The (002) peaks of the LCO epitaxial thin films on (001) STO substrates with the XRD $\theta/2\theta$ symmetric scans.

Table 1. The out-of-plane parameter (c_{film}) of LCO films with different annealing temperatures.

Annealing Temperature (°C)	500	600	700	800	900
c_{film} (Å)	3.808 (1)	3.792 (4)	3.782 (7)	3.782 (0)	3.781 (3)

The morphological characteristics of the LCO thin films were carried out via a SEM. Figure 2a–d shows the surface morphology of LCO films annealed at 500, 600, 700, and 900 °C, respectively. It is found that the LCO film becomes denser with less grain boundary by increasing the annealing temperature. This result illustrates that the crystallinity of films could be improved by increasing the annealing temperature. Generally, the atomic force microscope AFM is a very effective method to explore the surface roughness on the nanometer scale and the surface morphology of thin films. To further confirm the crystal quality of LCO films, the AFM characterizations were involved in this study. The two-dimensional (2D) and three-dimensional (3D) surface topography of the LCO thin film with an annealing temperature of 900 °C are presented in Figure 3. The average roughness (Ra) of the surface for the LCO film annealed at 900 °C is only ~5.3 nm. Combining the above results, it is conclusive that the film quality could be improved by increasing the annealing temperature. This method could serve as a simple and efficient way to obtain high-quality epitaxial perovskite oxide films.

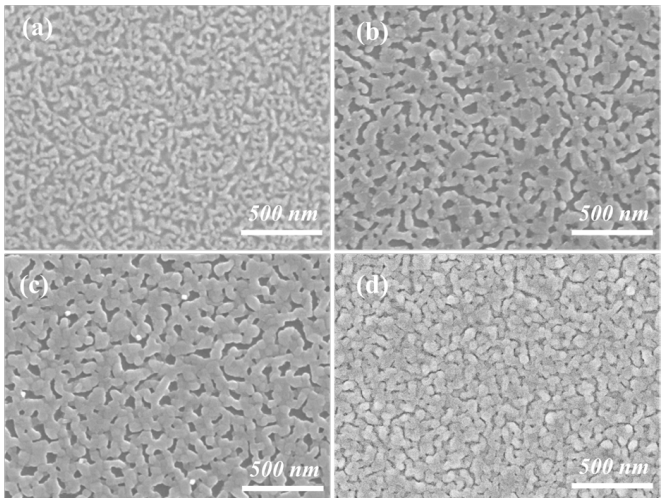

Figure 2. (Color online) The SEM micrographs of the LCO/STO thin films annealed at different temperatures: (**a**) 500 °C, (**b**) 600 °C, (**c**) 700 °C, and (**d**) 900 °C, respectively.

3.2. Thermal Decomposition Characteristics of 50% PEI

Due to the strong coordination reaction ability of PEI in the solution, the small metal chelate in the solution is firmly "bound" to the dendritic molecules of PEI, resulting in a homogeneous distribution of metal precursors and hence the formation of uniform metal-organic films. At the same time, PEI plays a protective role, avoiding the hydrolysis reaction of the metal cation in the precursor solution. Thus, the stability of the solution and the controllability of the reaction is improved, which play an important role in improving the quality of film crystallization. To figure out the reason why the annealing temperature has great influences on the crystallization quality, thermal decomposition experiments on a 50% PEI solution were carried out. As shown in Figure 4, the thermogravimetric analysis (TGA) curve goes through three major loss zones in the whole test temperature range. Regions from room temperature to 150, 250~350, and 400~700 °C correspond to the water loss of the free water and crystal water, fracture decomposition of the polymer chain, and volatilization of residues, respectively. In addition, there is an exothermic peak

around 332 °C in the differential scanning calorimetry (DSC) curve, indicating that the main obvious decomposition starts from this temperature.

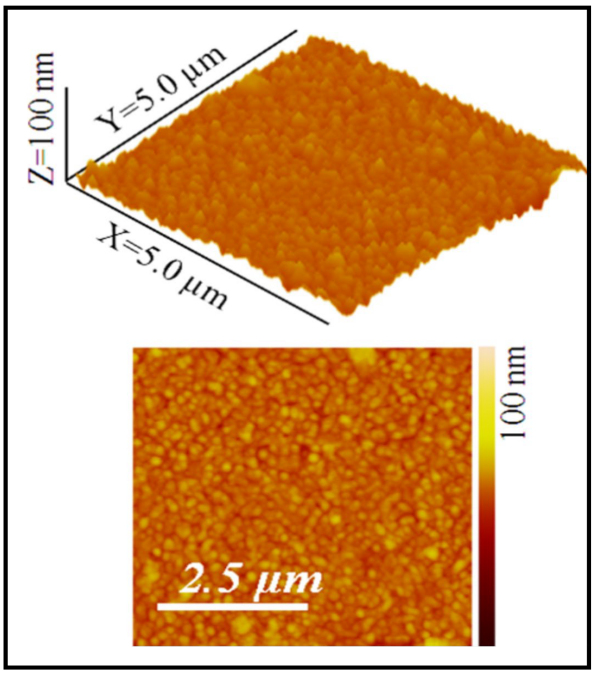

Figure 3. (Color online) Two-dimensional and three-dimensional AFM micrographs of LCO thin film deposited on STO with an annealing temperature of 900 °C.

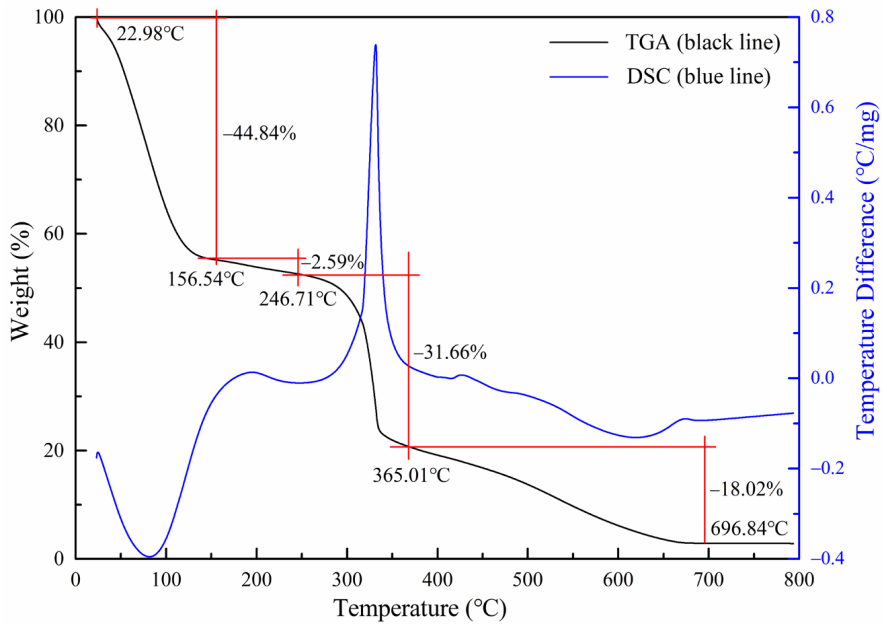

Figure 4. (Color online) The thermal decomposition data of 50% PEI solution.

As shown in the TGA and DSC curves, the decomposed temperature of the PEI is very wide, and PEI decomposes completely until the temperature reaches 700 °C. Therefore, to obtain high-quality LCO films, the annealing temperature should be controlled with a temperature above 700 °C, and the speed during the heat-up process should not be too fast. A high annealing temperature above 700 °C ensures the complete decomposition of the polymer and could prevent cracks in the film. Combining the thermal decomposition data and the X-ray diffraction data, we verified that appropriately raising the annealing

temperature facilitates the entire decomposition of PEI and the phase formation of LCO. This could serve as a guideline to improve the crystallization quality of epitaxial thin films.

3.3. The Structural and Epitaxial Properties of $La_{0.8}Sr_{0.2}CoO_3$ Films

Besides the influence of the annealing temperature, the strain is another important factor in structure and property control. The substitution of A-site ions of perovskite films not only changes the internal strain state but also vary the valence state of B-site ions. Thus Sr-doping $La_{0.8}Sr_{0.2}CoO_3$ (LSCO) grown on (001), (011), and (111)-oriented STO were prepared by the PAD method. The results of XRD $\theta/2\theta$ symmetric scans and ω scans for the epitaxial LSCO films are shown in Figure 5. Only (002), (011), and (111) peaks of LSCO films are observed without any undesirable peak from XRD patterns, indicating that the LSCO films have a preferential (001), (011), and (111) orientation, respectively.

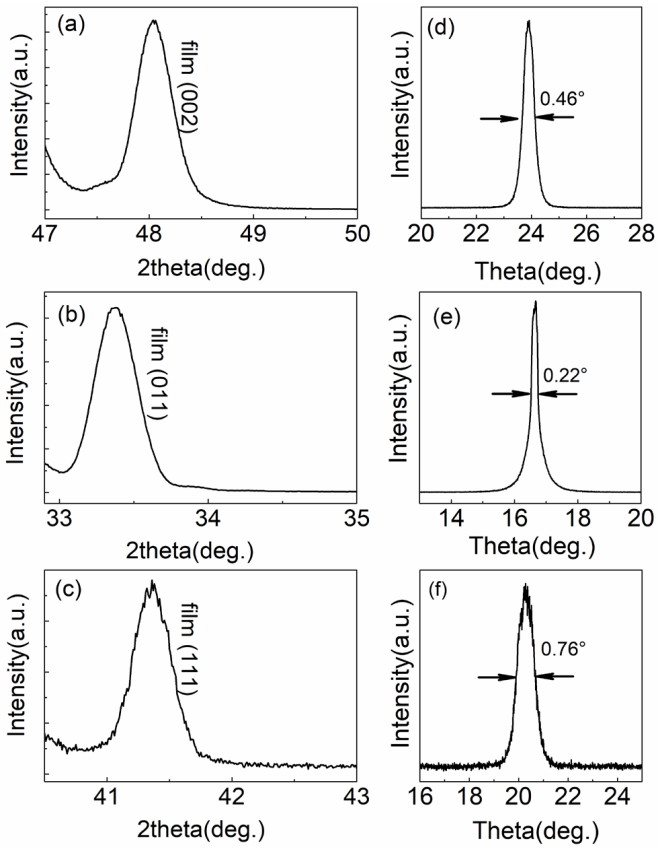

Figure 5. (**a**–**c**) The XRD $\theta/2\theta$ symmetric scans for LSCO thin films grown on (001) $SrTiO_3$, (011) $SrTiO_3$, and (111) $SrTiO_3$ substrates, respectively. (**d**–**f**) The rocking curves of Bragg peaks in Figure 5**a**–**c**, respectively. The arrows indicate the location and full width of the rocking curves at half maximum.

The in-plane symmetry was evaluated by the XRD φ scan (asymmetric Bragg reflection) for (101) reflections of the (001)-oriented LSCO thin films and the (001)-oriented STO substrate, as shown in Figure 6. Diffraction peaks with four-fold symmetry are observed for both the film and substrate. These results indicate that the LSCO film is epitaxially grown on the (001) STO substrate as a "cube-on-cube" mode [20]. The epitaxial relationship between the LSCO films and the STO substrate is confirmed to be (001) LSCO||(001) STO and (100) LSCO||(100) STO. The in-plane symmetry analysis of LSCO thin films grown on (011) and (111)-oriented STO was also carried out and presented similar results in our previous report [17], which is not shown here. According to the above results, the orientation of the LSCO films is consistent with that of the corresponding substrates.

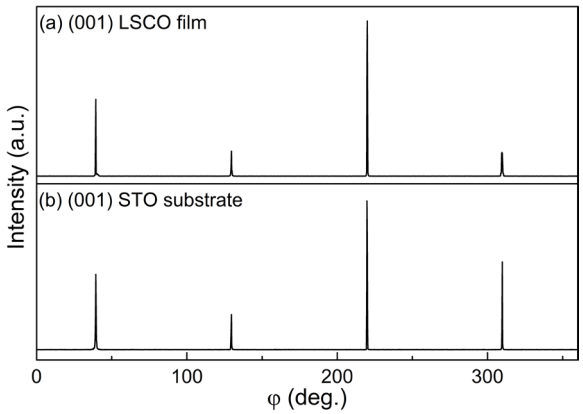

Figure 6. The in-plane φ-scans at (101) reflections of (**a**) LSCO thin film and (**b**) the (001) STO substrate.

Figure 5d–f exhibits the rocking curve of LSCO films grown on different STO substrates. The FWHM (full width at half maximum) values for the samples are less than 0.8°, suggesting the high quality of the LSCO films. The out-of-plane lattice parameters of (001), (011), and (111)-oriented LSCO films are calculated and listed in Table 2. The lattice parameter c_{film} of LSCO film grown on (001) STO is calculated to be 3.785(4) Å, a value larger than that of undoped LCO film with an annealing temperature of 900 °C (see Table 1). This result is mainly due to the bigger ionic radius of Sr^{2+} compared with La^{3+}. The larger c_{film} of the LSCO film also gives an indication that the Sr^{2+} ions were successfully doped into LCO.

Table 2. Out-of-plane (c_{film}) and biaxial strain (ε) of the LSCO epitaxial thin film. The pseudocubic lattice parameters of bulk LSCO are $a_{\text{bulk}} \approx 3.82$ Å, 2.701 Å, and 2.205Å, respectively.

Orientation	a_{bulk} (Å)	*Substract* a_s (Å)	c_{film} (Å)	ε (%)
(001)	3.820	3.905	3.785 (4)	−0.92
(011)	2.701	2.761	2.685 (1)	−0.60
(111)	2.205	2.254	2.183 (2)	−1.00

It is known that bulk LSCO crystalizes in a pseudocubic perovskite structure with a lattice parameter of $a_{\text{bulk}} \approx 3.82$Å. The theoretical values of out-of-plane lattice parameters are about 2.701Å and 2.205Å for (011) and (111)-oriented LSCO, respectively. Obviously, parameter c_{film} shown in Table 2 is less than those of the pristine bulk LSCO, which indicate that the film is successfully epitaxial on the substrate. Compared with the bulk LSCO, the LSCO films grown on STO substrates are subjected to the biaxial stretching strain in the *ab* plane (parallel to the film surface). This results in the compression along the *c*-axis and the distortion of CoO_6 regular octahedrons. Due to the larger lattice parameter of the STO substrate, the LSCO films possess larger lattice parameters and favor the high-spin state compared to bulk LSCO. According to the previous report, the compressive effect along the vertical direction in (011) and (111)-oriented LCO films is smaller than that in (001)-oriented LCO films [21]. However, in this work, the out-of-plane strain for (011)-oriented LSCO is smaller than that in (001) and (111)-oriented LSCO. This result implies that (011)-oriented LSCO films have an in-plane lattice relaxation.

3.4. The Spin State and Magnetic Transport Properties of LCO and LSCO Films

To find the effect of orientation and Sr doping on the magnetic properties and ground state, we measured the susceptibility of LCO and LSCO samples. Figure 7a,b shows the temperature-dependent magnetization of the (001), (011), and (111)-oriented LSCO thin films with an external magnetic field of H = 100Oe applied parallel to the film surface. The three LSCO films with different orientations show ferromagnetic transitions with the Curie temperature T_C at about 130, 162, and 158 K, respectively. Here the T_C is determined

by the minimum of the derivative of the FC magnetization (dM/dT) [20]. While for the LCO epitaxial film, the Curie temperature is observed to be ~ 83K, as shown in Figure 7c,d. Compared with pristine LCO films, the magnetic transition temperature of the Sr doping LSCO films is highly improved. Recently, Liu et al. studied the relationship between strain-induced structural modifications and the magnetic behaviors in $LaCoO_3$ thin films grown on various substrates [22]. Combining experimental results from Liu et al. and this study, it can be seen that chemical doping is an effective method to tune the physical properties of this system.

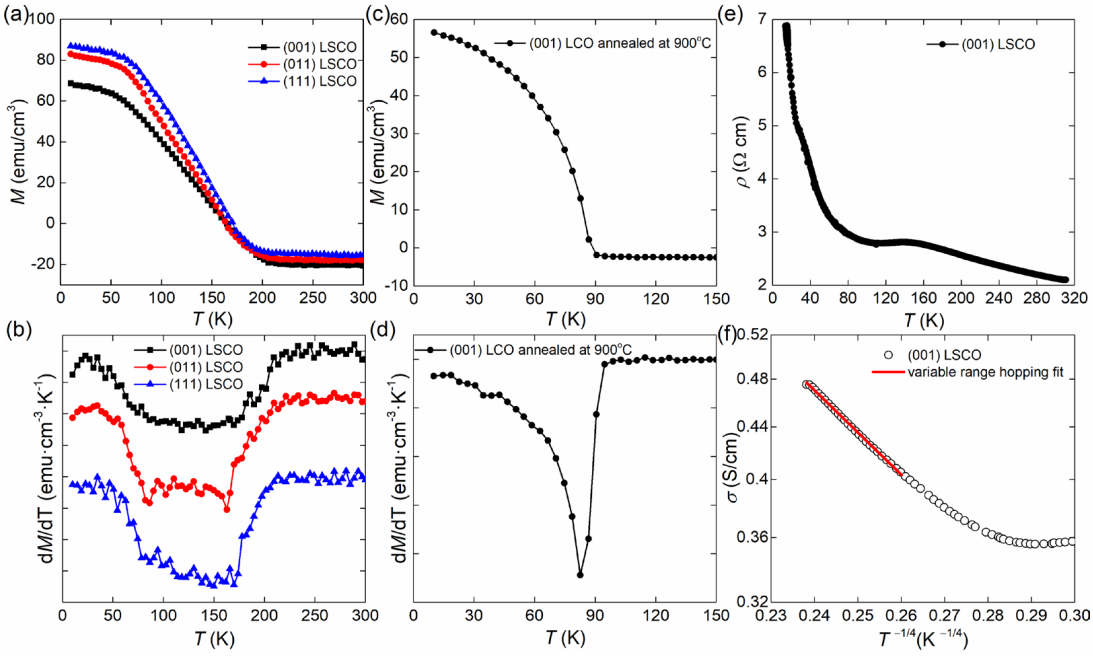

Figure 7. (Color online) (**a**) Temperature dependence of the LSCO magnetization (M vs. T) with an external magnetic field H = 100 Oe parallel to the film surface; (**b**) Temperature dependence of the differential magnetization of the LSCO. The curves are shifted, in turn, for clarity. (**c**) Temperature dependence of the LCO magnetization. (**d**) Temperature dependence of the differential magnetization of the LCO. (**e**) Temperature-dependent resistivity of the (001)-orientated LSCO film. (**f**) Temperature-dependent conductivity of the (001)-orientated LSCO film. The vertical coordinate is in the log scale.

According to previous reports, spin-lattice coupling is a common interaction in cobaltites [23,24]. It gives rise to phase separations in related materials. For bulk $La_{1-x}Sr_xCoO_3$ with doping levels of up to x = 0.5, hole-rich ferromagnetic regions, spin-glass regions, and hole-poor low spin regions coexist and compete with each other [25–27]. The joint effects of the former two regions result in broad ferromagnetic transitions. Similar behavior also appears in LSCO films in this study; the ferromagnetic transition goes through a wide temperature interval from ~190 to ~60 K, as shown in Figure 7a,b. This phenomenon reveals possible inhomogeneous ground states in LSCO films grown on STO.

Actually, the cases in LSCO films are different from that in LCO films. First, the Sr substitution changes the valence state of Co and introduces Co^{4+}. In epitaxial perovskite cobalt oxides, ferromagnetism derives from double exchange interactions. The formation of Co^{4+}–O–Co^{3+} changes the strength of the exchange interaction and modifies the Curie temperature in this system. Secondly, besides epitaxial strains, there are additional chemical strains deriving from Sr doping in LSCO films. This is expected to bring about changes in the strength of the Jahn–Teller effect, Co–O distance r_{Co-O}, and Co–O–Co angle θ. The spin state will also be modified accordingly, which might be another reason causing the enhanced ferromagnetism in LSCO (T_c~162K) compared with LCO (T_c~85K) [22].

In general, the spin-state transition of Co^{3+} results from a competition between crystal-field splitting (Δ_{CF}) and Hund's exchange energy (Δ_{ex}). Here, Δ_{CF} is the splitting between

the e_g and t_{2g} energy levels of Co $3d^6$ electron configuration, Δ_{ex} is the intra-atomic exchange interaction, which leads to a redistribution of electrons between e_g and t_{2g} energy levels, respectively. In a simple crystal-field picture for a regular CoO_6 octahedron in pristine LCO, the low-spin state is stable if $\Delta_{CF} > \Delta_{ex}$, whereas a higher spin state dominates if $\Delta_{CF} < \Delta_{ex}$. Owing to the overlap of Co (3*d*)-derived e_g and O (2*p*) orbits, the e_g-t_{2g} gap will be further narrowed. Thus Δ_{CF} expressed as $\Delta_{CF} - W/2$ is more accurate, where W is the bandwidth of the *d*-*p* bands [20,28]. On the other hand, since $W \propto r_{Co\text{-}O}{}^{-3.5} \sin(\theta/2)$ and $\Delta_{CF} \propto r_{Co\text{-}O}{}^{-5}$ [28], it can be concluded that the high-spin state is increased by an increase in $r_{Co\text{-}O}$ and θ in LSCO films. Consequently, the enhanced ferromagnetism in LSCO films is mainly associated with the doping-induced Co^{4+}–O–Co^{3+} configurations and Co spin-state transition [23,24,27].

To further characterize the Sr-doped films, the temperature dependence of the resistivity curve was measured and shown in Figure 7e. A resistive kink appears at ~150 K, which is consistent with the ferromagnetic transition shown in the magnetic measurements. This behavior indicates that the spins and charges are coupled with each other in this system. Figure 7f exhibits the transport behavior in the form of σ vs. $T^{-1/4}$. In the high-temperature region, the curve could be well described by the variable range hopping mechanism, the expression of which is $\sigma \propto \exp\left(-B/T^{1/4}\right)$. This illustrates that disorders such as grain boundaries and vacancies might exist in this material.

4. Conclusions

In summary, the high-quality LCO and LSCO thin films with different orientations were deposited on the STO substrates by a PAD method. Structural and morphological characterizations of LCO films were carried out. The results indicate that appropriately increasing the annealing temperature is helpful in improving the film crystallinity. The thermal decomposition measurements of 50% PEI verified that better crystallinity is attributed to the higher oxygen pressure and complete decomposition of PEI during the annealing process. The lattice parameter c_{film} of (001)-oriented $La_{0.8}Sr_{0.2}CoO_3$ film is larger than that of the LCO film, which is derived from the larger ionic radius of doping Sr^{2+} ions and the epitaxial strain induced by STO. Another effect caused by Sr doping is the introduction of Co^{4+} that results in Co^{3+}–O–Co^{4+} double exchange interaction, which further leads to the tendency that LSCO films favor staying in the high-spin state. Therefore, the changes in spin state for Co ions and the formation of Co^{3+}–O–Co^{4+} double exchange are responsible for the enhanced magnetic interaction in LSCO films, which further leads to an apparently higher transition temperature T_c in $La_{0.8}Sr_{0.2}CoO_3$ compared to pristine $LaCoO_3$ films. In addition, a highly inhomogeneous ground state induced by Sr doping results in a wide ferromagnetic transition zone. This study reveals that the annealing temperature and the orientations of substrates are key factors influencing the physical properties of epitaxial perovskite films.

Author Contributions: Methodology, C.X.; validation, C.X. and Y.M.; formal analysis, C.X.; investigation, C.X., Z.C. and X.W.; data curation, C.X. and Y.M.; writing—original draft preparation, C.X.; writing—review and editing, C.X. and Y.W.; supervision, Y.M.; project administration, C.X.; funding acquisition, C.X., Y.M. and Y.W. All authors have read and agreed to the published version of the manuscript.

Funding: This research was supported by the National Natural Science Foundation of China grant number 12204486, Anhui Provincial Natural Science Foundation grant number 2208085QA15, the Scientific Research Project of Higher Education in Anhui Province grant numbers 2022AH052125 and KJ2021A0912, the Universities Joint Key Laboratory of Photoelectric Detection Science and Technology in Anhui Province grant number 2020GDTC02, the Scientific Research Start-up Fund for Introduction of High-level Talents of HFNU grant number 2020rcjj09, the China Postdoctoral Science Foundation grant number 2020M682055, the Anhui Postdoctoral Foundation grant number 2021B508, the HFIPS Director's Fund grant number YZJJ2021QN30, the R&D Project for Qingdao

XITE CARBON Co., Ltd. grant number HXXM2022043, and the R&D Project for Hefei Yuwang Membrane Engineering Technology Co., Ltd. grant number HXXM2022239.

Data Availability Statement: The experimental data is available from the corresponding authors on reasonable request.

Conflicts of Interest: The authors declare no conflict of interest.

References

1. Chen, J.; Mao, W.; Gao, L.; Yan, F.; Yajima, T.; Chen, N.; Chen, Z.; Dong, H.; Ge, B.; Zhang, P.; et al. Electron-Doping Mottronics in Strongly Correlated Perovskite. *Adv. Mater.* **2019**, *32*, 1905060. [CrossRef] [PubMed]
2. Bristowe, N.C.; Varignon, J.; Fontaine, D.; Bousquet, E.; Ghosez, P. Ferromagnetism induced by entangled charge and orbital orderings in ferroelectric titanate perovskites. *Nat. Commun.* **2015**, *6*, 6677. [CrossRef]
3. Li, J.; Green, R.J.; Zhang, Z.; Sutarto, R.; Sadowski, J.T.; Zhu, Z.; Zhang, G.; Zhou, D.; Sun, Y.; He, F.; et al. Sudden collapse of magnetic order in oxygen deficient nickelate films. *Phys. Rev. Lett.* **2021**, *126*, 187602. [CrossRef] [PubMed]
4. Chen, J.; Mao, W.; Ge, B.; Wang, J.; Ke, X.; Wang, V.; Wang, Y.; Döbeli, M.; Geng, W.; Matsuzaki, H.; et al. Revealing the role of lattice distortions in the hydrogen-induced metal-insulator transition of $SmNiO_3$. *Nat. Commun.* **2019**, *10*, 694. [CrossRef]
5. Seyfi, B.; Baghalha, M.; Kazemian, H. Engineering Oxygen Vacancies into $LaCoO_3$ Perovskite for Efficient Electrocatalytic Oxygen Evolution. *Chem. Eng. J.* **2019**, *148*, 306–311. [CrossRef]
6. Wang, M.; Han, B.; Deng, J.; Jiang, Y.; Zhou, M.; Lucero, M.; Wang, Y.; Chen, Y.; Yang, Z.; N'Diaye, A.T.; et al. Influence of Fe Substitution into $LaCoO_3$ Electrocatalysts on Oxygen-Reduction Activity. ACS Appl. *Mater. Interfaces* **2019**, *11*, 5682–5686. [CrossRef] [PubMed]
7. Fuchs, D.; Pinta, C.; Schwarz, T.; Schweiss, P.; Nagel, P.; Schuppler, S.; Schneider, R.; Merz, M.; Roth, G.; Löhneysen, H.v. Ferromagnetic order in epitaxially strained $LaCoO_3$ thin films. *Phys. Rev. B* **2007**, *75*, 144402. [CrossRef]
8. Herklotz, A.; Rata, A.D.; Schultz, L.; Dörr, K. Reversible strain effect on the magnetization of $LaCoO_3$ films. *Phys. Rev. B* **2009**, *79*, 092409. [CrossRef]
9. Park, S.; Ryan, P.; Karapetrova, E.; Kim, J.W.; Ma, J.X.; Shi, J.; Freeland, J.W.; Wu, W. Microscopic evidence of a strain-enhanced ferromagnetic state in $LaCoO_3$ thin films. *Appl. Phys. Lett.* **2009**, *95*, 072508. [CrossRef]
10. Fuchs, D.; Dieterle, L.; Arac, E.; Eder, R.; Adelmann, P.; Eyert, V.; Kopp, T.; Schneider, R.; Gerthsen, D.; Lohneysen, H.v. Suppression of the ferromagnetic state in $LaCoO_3$ films by rhombohedral distortion. *Phys. Rev. B* **2009**, *79*, 024424. [CrossRef]
11. Choi, W.S.; Kwon, J.-H.; Jeen, H.; Hamann-Borrero, J.E.; Radi, A.; Macke, S.; Sutarto, R.; He, F.; Sawatzky, G.A.; Hinkov, V.; et al. Strain-Induced Spin States in Atomically Ordered Cobaltites. *Nano Lett.* **2012**, *12*, 4966–4970. [CrossRef] [PubMed]
12. Liu, G.; Li, X.; Wang, Y.; Liang, W.; Liu, B.; Feng, H.; Sun, J. Nanoscale domains of ordered oxygen-vacancies in $LaCoO_3$ films. *Appl. Surf. Sci.* **2017**, *425*, 121–129. [CrossRef]
13. Zhang, N.; Zhu, Y.; Li, D.; Pan, D.; Tang, Y.; Han, M.; Ma, J.; Wu, B.; Zhang, Z.; Ma, X. Oxygen Vacancy Ordering Modulation of Magnetic Anisotropy in Strained $LaCoO_{3-x}$ Thin Films. *ACS Appl. Mater. Interfaces* **2019**, *10*, 38230–38238. [CrossRef] [PubMed]
14. Zhu, L.; Chen, S.; Zhang, H.; Zhang, J.; Sun, Y.; Li, X.; Xu, Z.; Wang, L.; Sun, J.; Gao, P.; et al. Strain-inhibited electromigration of oxygen vacancies in $LaCoO_3$. ACS Appl. *Mater. Interfaces* **2019**, *11*, 36800–36806. [CrossRef] [PubMed]
15. Ajmal, S.; Bibi, I.; Majid, F.; Ata, S.; Kamran, K.; Jilani, K.; Nouren, S.; Kamal, S.; Ali, A.; Iqbal, M. Effect of Fe and Bi doping on $LaCoO_3$ structural, magnetic, electric and catalytic properties. *J. Mater. Res. Technol.* **2019**, *8*, 4831–4842. [CrossRef]
16. Shin, D.; Yoon, S.; Song, S.; Park, S.; Lee, H.N.; Choi, W.S. Tunable ferromagnetism in $LaCoO_3$ epitaxial thin films. *Adv. Mater. Interfaces* **2022**, *9*, 2200433. [CrossRef]
17. Xie, C.; Shi, L.; Zhao, J.; Zhou, S.; Li, Y.; Guo, J. Insight into the enhancement of transport property for oriented $La_{0.9}MnO_3$ films. *J. Phys. D Appl. Phys.* **2017**, *50*, 205306. [CrossRef]
18. Ridha, S.; Essebti, D.; Hlil, K. Impact of annealing temperature on the physical properties of the lanthanum deficiency manganites. *Crystals* **2017**, *7*, 301. [CrossRef]
19. Xie, C.; Shi, L.; Zhao, J.; Li, Y.; Zhou, S.; Yao, D. The influence of substrate orientation and annealing condition on the properties of $LaMnO_3$ thin films grown by polymer-assisted deposition. *Appl. Surf. Sci.* **2015**, *351*, 188–192. [CrossRef]
20. Fuchs, D.; Arac, E.; Pinta, C.; Schuppler, S.; Schneider, R.; Löhneysen, H.v. Tuning the magnetic properties of $LaCoO_3$ thin films by epitaxial strain. *Phys. Rev. B* **2008**, *77*, 014434. [CrossRef]
21. Liu, H.; Shi, L.; Guo, Y.; Zhou, S.; Zhao, J.; Wang, C.; He, L.; Li, Y. Nature of ferromagnetic ordered state in $LaCoO_3$ epitaxial nano-thin film on $LaAlO_3$ substrate. *J. Alloys Compd.* **2014**, *594*, 158–164. [CrossRef]
22. Liu, H.; Shi, L.; Zhou, S.; Zhao, J.; Guo, Y.; Wang, C.; He, L. Simple polymer assisted deposition and strain-induced ferromagnetism of $LaCoO_3$ epitaxial thin films, Surf. *Coat. Technol.* **2013**, *226*, 108–112. [CrossRef]
23. Kuhns, P.L.; Hoch, M.J.R.; Moulton, W.G.; Reyes, A.P.; Wu, J.; Leighton, C. Magnetic phase separation in $La_{1-x}Sr_xCoO_3$ by ^{59}Conuclear magnetic resonance. *Phys. Rev. Lett.* **2003**, *91*, 127202. [CrossRef] [PubMed]
24. Hoch, M.J.R.; Kuhns, P.L.; Moulton, W.G.; Reyes, A.P.; Lu, J.; Wu, J.; Leighton, C. Evolution of the ferromagnetic and nonferromagnetic phases with temperaturein phase-separated $La_{1-x}Sr_xCoO_3$ by high-field 139La NMR. *Phys. Rev. B* **2004**, *70*, 174443. [CrossRef]

25. Nam, D.N.H.; Jonason, K.; Nordblad, P.; Khiem, N.V.; Phuc, N.X. Coexistence offerromagnetic and glassy behavior in the $La_{0.5}Sr_{0.5}CoO_3$ perovskitecompound. *Phys. Rev. B* **1999**, *59*, 4189. [CrossRef]
26. Wu, J.; Leighton, C. Pressure-inducedinsulating state in (La,Sr)CoO_3. *Phys. Rev. B* **2003**, *67*, 174408. [CrossRef]
27. Fita, I.; Szymczak, R.; Puzniak, R.; Wisniewski, A.; Troyanchuk, I.O.; Karpinsky, D.V.; Markovich, V.; Szymczak, H. Ferromagnetic state of $La_{1-x}Ba_xCoO_3$ under applied pressure: Factors controlling the sign reversal of pressure effect in cobaltites. *Phys. Rev. B* **2011**, *83*, 064414. [CrossRef]
28. Sterbinsky, G.E.; Ryan, P.J.; Kim, J.-W.; Karapetrova, E.; Ma, J.X.; Shi, J.; Woicik, J.C. Local atomic and electronic structures of epitaxial strained $LaCoO_3$ thin films. *Phys. Rev. B* **2012**, *85*, 020403. [CrossRef]